Limnology and Oceanography
FLUIDS & ENVIRONMENTS

ORIGINAL ARTICLE

Lagrangian transport pathways in the northeast Atlantic and their environmental impact

Iria Sala,[1] **Rui M. A. Caldeira,**[1,2] **Sheila N. Estrada-Allis,**[3] **Elsa Froufe,**[1] **and Xavier Couvelard**[2]

Abstract

*This study focused on mapping the general transport pathways of the northeast Atlantic Ocean by using the Regional Oceanic Modeling System to calculate ocean current velocity components (*u, v, w*), and Ariane (an off-line Fortran code dedicated to the computation of three-dimensional streamlines from velocity fields) to calculate the transport of particles around the numerical model domain. The study was undertaken using a 10-year climatic simulation. Statistical comparisons with satellite and in situ data showed that the ocean circulation model captured known regional oceanographic features. Four depth ranges showed different Lagrangian transport pathways, 0–10 m, 20–200 m, 300–500 m, and 600–2000 m, confirming that these routes are consistent with the known ocean circulation patterns. Our results were supported by multiple sources: (i) connectivity between the African coast and the Canary Islands for sardine (*Sardina pilchardus*), anchovy (*Engraulis encrasicolus*), (ii) panmixia of lobsters (*Scyllarides latus *and* Palinurus elephas*), and European conger eel (*Conger conger*); (iii) connectivity between Azores and Canary archipelagos for sponge (*Phorbas fictitius*); and (iv) observed drifting of crude oil from the *Prestige* oil tanker spill. These results should help guide future observational campaigns, as well as the interpretation of open-ocean transport patterns and the distribution of marine organisms and chemical tracers in the northeast Atlantic region.*

Keywords: drifting, rafting, connectivity, pollutant and larval transport, water masses

[1]Centro Interdisciplinar de Investigação Marinha e Ambiental, Universidade do Porto, Porto, Portugal

[2]Centro de Ciências Matemáticas, Universidade da Madeira, Funchal, Portugal

[3]Universidad de Las Palmas de Gran Canaria, Las Palmas, Spain

Correspondence to Rui M. A. Caldeira rcaldeira@ciimar.up.pt

Introduction

[1] The northeast Atlantic Ocean (NEA), east of Mid-Atlantic Ridge, is characterized by the presence of the North Atlantic Current (NAC), Azores Current (AzC), and the Canary Current (CaC), all part of the eastern anticyclonic North Atlantic subtropical gyre (Fig. 1). The AzC is the southeastward branch of the Gulf Stream (e.g., Gould 1985), transporting warm and salty water across the Mid-Atlantic Ridge (~34° N, 37° W), southwest of the Azores Archipelago (AZ) (Käse and Siedler 1982; Gould 1985). Then, the AzC flows eastward toward the Gulf of Cádiz (Fernández and Pingree 1996; Martins et al. 2002), producing a front with significant temperature and salinity gradients (Käse et al. 1985). This front is characterized by complex mesoscale variability reflected by elevated eddy kinetic energy (EKE). An eastward branch of the AzC joins the CaC (New et al. 2001), north and around the Madeira Archipelago (MA), making the CaC

© 2013 by the Association for the Sciences of Limnology and Oceanography, Inc.

Downloaded by guest on May 26, 2013

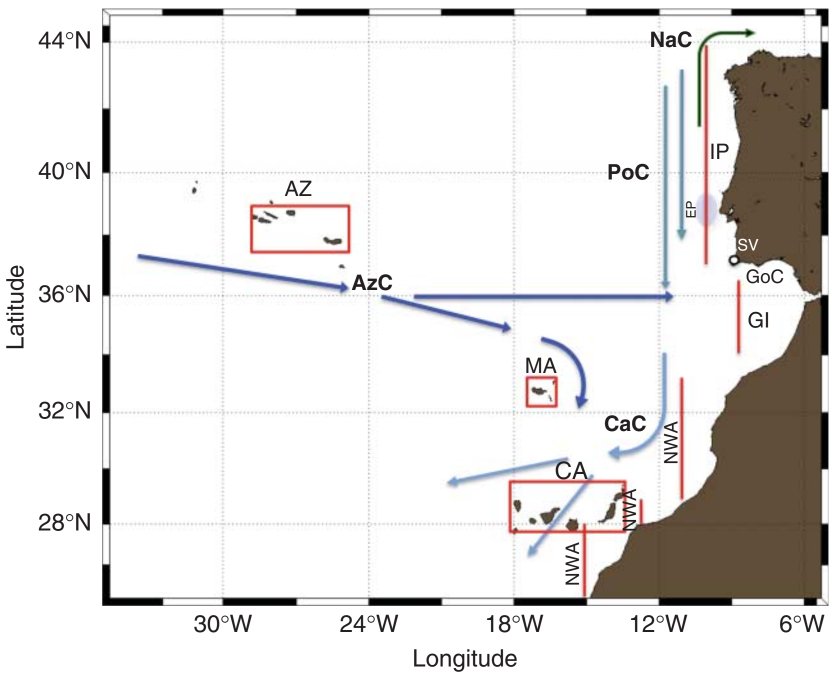

Fig. 1 The main large-scale surface currents in our study area are the Azores Current (AzC), the Canary Current (CaC), and the Portugal Current (PoC). The approximate location of the Navidad Current (NaC) is also shown. Red squares delimit source/sink areas around the Macaronesian islands: Azores Archipelago (AZ), Madeira Archipelago (MA), and Canary Archipelago (CA). The red meridional lines define coastal source/sink areas: the Iberian Peninsula (IP), Northwest African coast (NWA), and Strait of Gibraltar (GI). The locations of the Gulf of Cádiz (GoC), Cape St. Vicente (SV), and Estremadura Promontory (EP) are also noted.

a natural extension of the AzC. The CaC flows southward through the Canary Archipelago (CA), producing a large eddy field downstream of the archipelago (Barton et al. 2004). These eddies interact with coastally generated upwelling filaments, promoting offshore transport (e.g., Hernández-León et al. 2007; Rodríguez et al. 2009). The Portuguese Current (PoC) is a broad equatorward current that allows exchange between the NAC and the AzC (Dietrich et al. 1980); the CaC also receives a small contribution from the PoC (Barton et al. 2001). Below the mixed layer lies the high-salinity North Atlantic Central Water (NACW), with a lower limit at about 800 m depth (Hernández-Guerra et al. 2002). Below the NACW are the Mediterranean Water and the Intermediate Antarctic Water (Hernández-Guerra et al. 2003). The Mediterranean Intermediate Water (MIW) exits the Strait of Gibraltar (GI) and spreads over the northeastern part of the Gulf of Cádiz, moving downslope close to the bottom as a density current (e.g., Ambar and Howe 1979a, 1979b) while entraining NACW. Sy (1988) concluded from hydrographic observations near the Mid-Atlantic Ridge that the Mediterranean Water tongue slides westward between the two major zonal currents in the region, the NAC in the north and the AzC in the south.

[2] The North Atlantic upwelling region is one of the four major eastern boundary systems of the world, with a strong seasonal variability (e.g., Álvarez et al. 2009). It extends from Cape Finisterre (northwest of Spain; 43° N) to the south of Cape Verde (Senegal; 10° N). This upwelling region is characterized by slow, broad, equatorward gyre recirculation, a meridional alignment of coastlines, and a predominant equatorward wind direction during a substantial part of the year. A distinctive characteristic of this system is the discontinuity imposed by the entrance of the Mediterranean Sea, forming two distinct subsystems: the Canary Basin and the Iberian Peninsula (IP) (e.g., Barton 1998). Various oceanographic studies conducted in the Iberian system reveal a succession of mesoscale structures such as jets, meanders, ubiquitous eddies, upwelling filaments, and countercurrents, superimposed on the more stable variations at seasonal timescales (e.g., Serra and Ambar 2002; Peliz et al. 2005). In this area, we find the Macaronesian archipelagos (AZ, MA, and CA; Fig. 1), a group of volcanic islands thought to be of Miocene origin (Briggs 1970; Schmincke 1973). The AZ extends from west to east across the Mid-Atlantic Ridge. It is located 1584 km from the nearest continental margin (Portugal) and 860 km from the MA (Borges and Brown 1999). The AZ is bracketed to the south by AzC and to the north by the NAC. The MA has an intermediate geographical position between the AZ and CA. The MA lies within the main eastward flow of the AzC. The CA is located between 100 and 500 km from the African coast. This

© 2013 by the Association for the Sciences of Limnology and Oceanography, Inc. / e-ISSN 2157-3689

Downloaded by guest on May 26, 2013

archipelago, due to its geographical position, acts as a barrier to the incoming CaC.

[3] The aim of this study is to map the most probable transport routes in the NEA, applying a Lagrangian off-line numerical tool (Ariane) attached to a validated ocean circulation model. The routes were defined after analyzing the trajectories followed by a set of particles arranged at different source areas and depths over a 10-year simulation. These paths could provide an initial view of connectivity in the NEA, but it was necessary first to carry out a background study to map the general transport pathways in the region by keeping released particles at constant depths. Whereas Sangrà et al. (2009) discussed the westward propagation induced by oceanic eddies, the general transport pathways in the NEA circulation have not been fully addressed. Identifying such routes should inform larval transport and genetic connectivity studies (e.g., Cowen and Sponaugle 2009; Watson et al. 2010; Brochier et al. 2011) and improve our understanding of the transport of contaminants (e.g., González et al. 2008), the identification and tracking of water masses (Izumo et al. 2002; Koch-Larrouy et al. 2010), and the validation of numerical models (e.g., van Sebille et al. 2009).

Model Description

The Regional Ocean Circulation Numerical Modeling System

[4] The Institut de Recherche pour le Développment (IRD) version of the Regional Oceanic Modeling System (ROMS, http://www.romsagrif.org) was used in this study (see Shchepetkin and McWilliams 2003, 2005). ROMS is a split-explicit, free-surface, and terrain-following vertical coordinate model. To encompass the most relevant dynamic features of the NEA region, taking into account previous studies of the Canary Basin ocean circulation, and considering the oceanographic data set available for model validation, an extended rectangular grid from 25° N to 45° N in latitude, and from 35° W to 5° W in longitude was considered. The model grid, atmospheric forcing, and initial and boundary conditions were built using the ROMSTOOLS package (Penven et al. 2008). The bottom topography was derived from a 30-arc-second resolution database, GEBCO_08 (http://www.gebco.net). To preserve a sufficient resolution in the upper ocean, we used 50 vertical levels with stretched *s*-coordinates (Song and Haidvogel 1994). The ROMS solution used in this study was forced with WOA05 climatology at the oceanic boundaries, and with COADS climatology (atmospheric heat and momentum; Da Silva et al. 1994). At the lateral boundaries facing the open ocean, a mixed passive-active, implicit radiation condition connects the model solution to the surroundings (Marchesiello et al. 2009). The model grid is eddy resolving with a 1/12° horizontal spatial resolution (i.e., about 8 km). Two years of spin-up were required to stabilize the volume-averaged kinetic energy inside the numerical domain. The solutions were computed for an additional 4 years, over which the statistical diagnostics for model-data validation were performed.

Validation of the Ocean Circulation Model

[5] To validate the regional model, a comparison of model solutions, satellite, and Argo (global array of temperature/salinity profiling floats) data was carried out. Root mean squared error (RMSE), coefficients of determination (r^2), and bias were computed at daily and weekly temporal scales for the entire domain. Generally, the regional model was in a good agreement with satellite data and Argo profiles (see Table 1 for a description of data used in the model validation). Main dynamical structures and water masses of NEA region were well represented by the regional solution.

Table 1 Details of the data products used in the validation of ROMS solution. AVHRR, Advanced Very High Resolution Radiometer data; AVISO, Archiving, Validation and Interpretation of Satellite Oceanographic data; EKE, eddy kinetic energy; MW, microwave; OI, optimally interpolated; SLA, sea level anomalies; SST, sea surface temperature.

Data	Source	Available time period	Spatial resolution	Temporal resolution
EKE from SLA	AVISO	2003–2006	1/3° × 1/3°	Weekly
SST	AVHRR-OI	Jan 1985 to present	1/4° × 1/4°	Daily
	MW-OI	Jun 2002 to present	1/4° × 1/4°	Daily
Temperature and salinity profiles	Argo floats	2003–2006	Irregular grid: 2057 profiles from 49 floats	

© 2013 by the Association for the Sciences of Limnology and Oceanography, Inc. / e-ISSN 2157-3689

Downloaded by guest on May 26, 2013

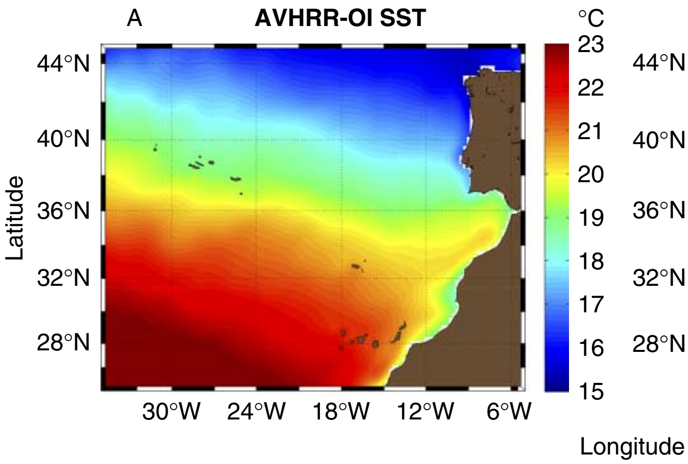

Fig. 2 Averaged (2003 – 2006) sea surface temperature (SST) for the study region: comparison between the Advanced Very High Resolution Radiometer (AVHRR) combined satellite data product (A) and the Regional Oceanic Modeling System (ROMS) solution (B).

[6] The north-south gradient of the sea surface temperature (SST) is an important feature in the NEA system. The general distribution of the SST model agreed well ($r^2 = 0.96$) with the AVHRR (Advanced Very High Resolution Radiometer) and MW-OI (Microwave Optimally Interpolated) combined and optimally interpolated satellite products of SST. Important NEA mesoscale structures, such as the Azores Front (AF), were well represented by the regional model. Comparisons with the MW-OI product showed quantitatively similar values for the model validation (Fig. 2).

[7] The EKE is a good proxy to represent the mesoscale variability associated with eddy activity (e.g., Le Traon and De Mey 1994; Volkov and Fu 2010). Fig. 3 compares the mean EKE field computed by the model with altimetry satellite data from AVISO (Archiving, Validation and Interpretation of Satellite Oceanographic) data. The best model representation is obtained in offshore regions. Furthermore, the lack of AVISO data near the coast favors comparison with offshore regions, since altimetry data accuracy is limited within 45 km of the coast (Durand et al. 2008). Higher RMSEs were found at strong dynamic areas such as the AF and the Gulf Stream (data not shown), where ROMS underestimated the EKE relative to the AVISO data.

[8] Argo buoy data were extracted for the 2003–2006 data set, during their trajectories in the NEA region (see subregions identified in Fig. 4). The main water

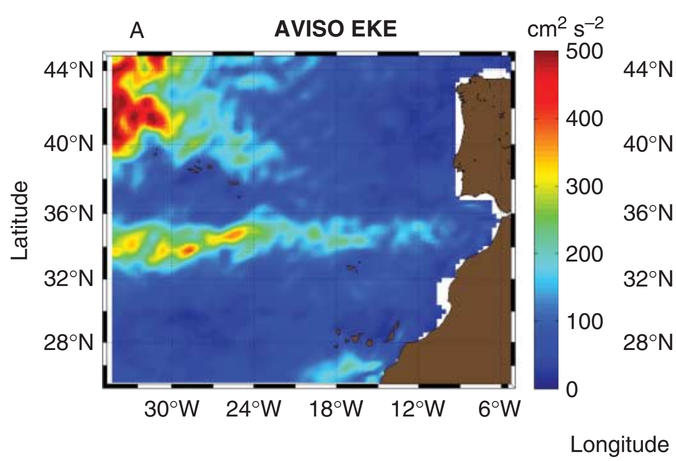

Fig. 3 Averaged (2003 – 2006) eddy kinetic energy (EKE; cm^2 s^{-2}): comparison between Archiving, Validation and Interpretation of Satellite Oceanographic (AVISO) altimetry data (A) and the Regional Oceanic Modeling System (ROMS) model solution (B).

© 2013 by the Association for the Sciences of Limnology and Oceanography, Inc. / e-ISSN 2157-3689

Downloaded by guest on May 26, 2013

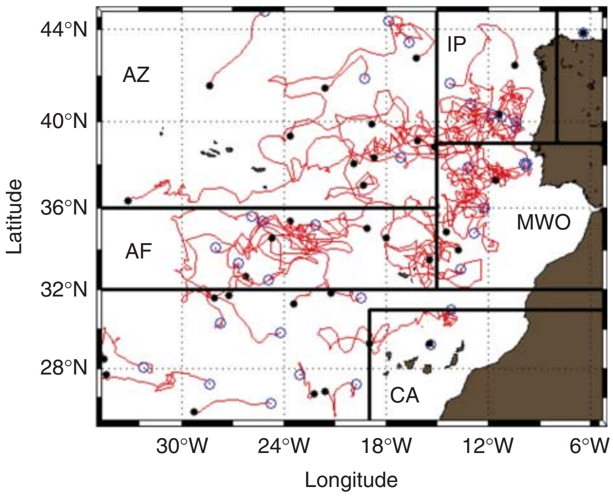

Fig. 4 Argo buoy trajectories (2003 – 2006 data set). Argo buoys oscillate between the surface and 2000 m every 10 d. They have sampled the water masses of the northeast Atlantic Ocean subregions: AZ, Azores Archipelago; AF, Azores Front; CA, Canary Archipelago; IP, Iberian Peninsula; and MWO, Mediterranean Water outflow. Blue circles represent the buoys' initial positions, and the black dots represent their final positions.

masses present in the study region were well reproduced by the regional model. In particular, the NACW (Fig. 5), characterized by density (σ) values of 27.38 kg m^{-3}, with potential temperature (θ) varying between 11 and 18°C and salinities varying between 35.5 and 36.5 psu was also reproduced by the model (e.g., Machín et al. 2006). The warmer and saltier MIW, characterized by σ varying between 27.38 and 27.92 kg m^{-3}, with $\theta = 10$°C, and salinities higher than 35.6 psu (e.g., Machín et al. 2006), was not represented by the model with the same accuracy. It must be emphasized that modeling the MIW is challenging due its particular mechanism of formation and dissipation through the Atlantic (e.g., Dietrich et al. 2008). In terms of the different NEA subregions, the best correlation was found for the AF subregion (Fig. 5B), with $r^2 = 0.99$ for temperature and $r^2 = 0.97$ for salinity. As expected, the lowest correlation is found in the Mediterranean Water Outflow (MWO) subregion (Fig. 5D), where r^2 were 0.94 and 0.86 for temperature and salinity, respectively. The results suggest that MIW salinity was somewhat underestimated in ROMS.

Ariane: The Offline Lagrangian Toolbox

[9] Ariane is a Lagrangian off-line numerical tool developed by Bruno Blanke and Nicolas Grima (Laboratoire de Physique des Océans; http://stockage.univ-brest.fr/~grima/Ariane/). It is written in Fortran, and it was developed to work with several ocean circulation model solutions such as ROMS. Ariane uses ROMS velocity fields (u, v, w) to compute the three-dimensional trajectories. The analysis was performed using the mass-preserving algorithm (Döös 1995; Blanke and Raynaud 1997; Blanke et al. 1999), which calculates true trajectories for a given stationary velocity field. Previous studies have successfully used Ariane to derive relevant information about basin-scale and global-scale circulation patterns (e.g., Blanke and Raynaud 1997; Blanke et al. 1999, 2001). Ariane has also been applied to biological problems to study larval transport and to identify spawning areas in a backward tracking mode, releasing particles in regions where populations were known to establish as adults (e.g., Bonhommeau et al. 2009; Pous et al. 2010).

[10] In the present study, Ariane was used to track passive particles from different release sites, at different depths, in order to map the main Lagrangian pathways in the NEA region. Table 2 summarizes the details of all simulations. Several sensitivity analyses were carried out in order to determine the seasonal and interannual variability: 1-year simulations were performed releasing particles around the Macaronesian islands (AZ, MA, and CA), along the IP coast, the GI, and along the northwest African (NWA) coast (see Fig. 1 for release/source areas) and at different constant depths (5, 100, 500, and 1000 m). In the sensitivity analysis of the seasonal variability, the particles were released in March, June, September, and December of year 1 (results are shown in Fig. 6). Meanwhile, in the interannual study, the particles were released on 1 January of each year of the 4-year ROMS solution (results are shown in Fig. 7). The preliminary tests suggested a small seasonal and interannual variability for the bulk transport of particles. Whereas individual particles can diverge in their trajectories across the ocean, in general most particles released from a common source region traveled similar routes. Considering that the 4-year ROMS solution was climatically forced, and the small interannual variability, we looped the 4-year ROMS solution 2.5 times to carry out a 10-year Lagrangian study with Ariane. This was important to model the displacement

© 2013 by the Association for the Sciences of Limnology and Oceanography, Inc. / e-ISSN 2157-3689

Downloaded by guest on May 26, 2013

of the particles released in slow-moving deep waters. Furthermore, Valdivieso Da Costa and Blanke (2004) suggested a minimum of 5 years to obtain accurate estimates of Lagrangian statistics. Considering the small seasonal variability during the study period, a single release event was considered (refer to Fig. 6 for sensitivity analysis). All particles were released on 1 January of year 1 and completed their travel on 31 December of year 10, or when they left the domain, or when they reached a (monitored) destination site. Throughout the 10-year simulation, the position of each particle was logged every day.

[11] We conducted a qualitative analysis (experiment 1) and a quantitative analysis (experiment 2) in the region. Experiment 1 was conducted to help identify the common depth ranges of the general Lagrangian routes by using particles that were released around the Macaronesian islands, along the IP coast, the GI, and along the NWA coast. To assess the effect of depth on transport routes, particles were released at 10-m depth intervals from the surface down to 100 m, at every 100 m thereafter down to 1000 m, and at 1200 m and 2000 m. These particles traveled in layers, that is, maintaining a constant depth, without being influenced by vertical transport to identify common pathways. After analyzing all the transport patterns, four representative depth ranges showed significantly different transport regimes: (1) 1–10 m, (2) 20–200 m, (3) 300–500 m, and (4) 600–2000 m. For each of these depth ranges, further

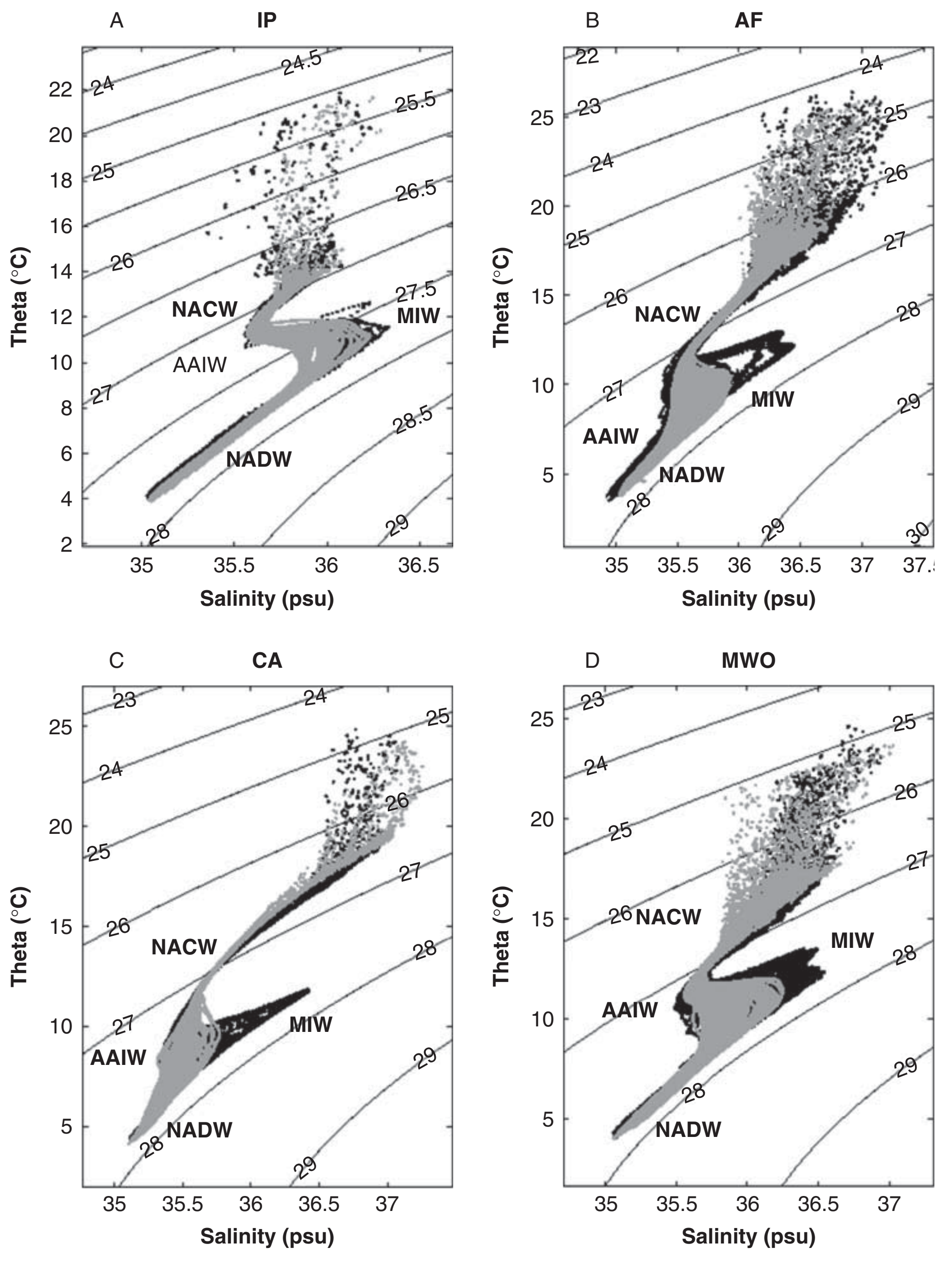

Fig. 5 Theta-s diagrams representing water mass characteristics from 0 to 2000 m depth and considering the Argo profiles (black lines) for the study period (2003–2006). Data from each subregion are plotted separately and compared with Regional Oceanic Modeling System (ROMS) model profiles (gray lines), considering the nearest location of each Argo profiles. A — Iberian Peninsula (IP) subregion considered data from 8 floats and 331 profiles. B — Azores Front (AF) subregion considered data from 8 floats and 446 profiles. C — Canary Archipelago (CA) subregion considered data from 2 floats and 57 profiles. D — Mediterranean Water Outflow (MWO) subregion considered data from 9 floats and 345 profiles. The profilers sampled the main water masses for the region: NADW, North Atlantic Deep Water; AAIW, Antarctic Intermediate Water; MIW, Mediterranean Intermediate Water; NACW, North Atlantic Central Water.

© 2013 by the Association for the Sciences of Limnology and Oceanography, Inc. / e-ISSN 2157-3689

Downloaded by guest on May 26, 2013

Table 2 Ariane simulation details.

	Simulations performed			
	Precision analyses (1 year)		Experiment (10 years)	
Depth (m)	Seasonal	Interannual	1: Qualitative	2: Quantitative
Surface water				
1			X	
5	X	X	X	X
10			X	
20			X	
30			X	
40			X	
50			X	
60			X	
70			X	
80			X	
90			X	
Intermediate water				
100	X	X	X	X
200			X	
300			X	
400			X	X
500	X	X	X	
600			X	
700			X	
800			X	
900			X	
Deep water				
1000	X	X	X	
1200				X
2000			X	

quantitative analyses were performed (experiment 2) to determine the physical connectivity between sources and sink sites. The same source and sink locations were considered (AZ, MA, CA, IP, GI, and NWA). The northern, southern, and western boundaries of our ROMS domain (NB, SB, and WB, respectively) were also added as sinks. The particles were released along the perimeter of a squared region circumscribing the Macaronesian archipelagos, from meridional transects along the continental coasts (Iberia and West Africa), and along the GI (see Fig. 1 for release sites). A total of 1002 particles where released at AZ and MA, 1018 particles from CA, and 1002 particles along the continental coast: 407 from IP, 137 from GI, and 458 from NWA. These particles were released across the depths identified in experiment 1 (1–10 m, 20–200 m, 300–500 m, and 600–2000 m). Sink areas at the model boundaries were set 2° away to avoid the influence of the "sponge layer" (layer characterized by enhanced viscosity/diffusion used to smooth minor inconsistencies between the evolving model solution and the external climatological data). The output files generated by Ariane include position (longitude, latitude, and depth) and time instance for each particle. Particles reached the sink location when they were inside the predefined (squared) regions or meridional coastlines or reached the boundaries of the numerical domain. During the 10-year simulation, some particles reached one sink and continued their journey onto other sinks. Nevertheless, no single particle was counted twice for the same sink, and the particles that crossed the NB, SB, and WB did not return into the domain. Therefore, during its travel, a single particle released in the AZ could reach MA, CA, and WB, and thus the overall counting may exceed 100%. Table 3 summarizes the results of the first quantitative study (experiment 2). Table 4 shows the travel time (days) for the first particles, and therefore the fastest ones, between sources and sinks. Fig. 8 shows the relationship between travel time of the fastest particle and distance traveled between sources and sink locations. As expected, particles released at surface waters (blue diamonds) traveled faster than the ones released in deep waters (purple circles). Particle routes at the different depth ranges are discussed further below.

Results

Lagrangian Transport Pathways of the NEA

Surface water routes, 1–10 m

[12] Most particles released in the AZ traveled southeast following the AzC, turning westward at the longitude of Madeira Island (Fig. 9A); 36.83% of particles released from the AZ reached the MA sink (Table 3A). At this depth range, the fastest particle reached Madeira Island in 332 d (Table 4A). The particles released around MA followed similar paths as the particles released in the AzC, with 23.35% of them reaching the CA (Fig. 9A; Table 3A). Considering MA as the source region, the fastest particle reached the CA in 101 d, whereas it took 767 d to reach the CA from the AZ (Table 4A). Thereafter, the trajectories of particles released at AZ and MA joined with the particles released at CA,

© 2013 by the Association for the Sciences of Limnology and Oceanography, Inc. / e-ISSN 2157-3689

Downloaded by guest on May 26, 2013

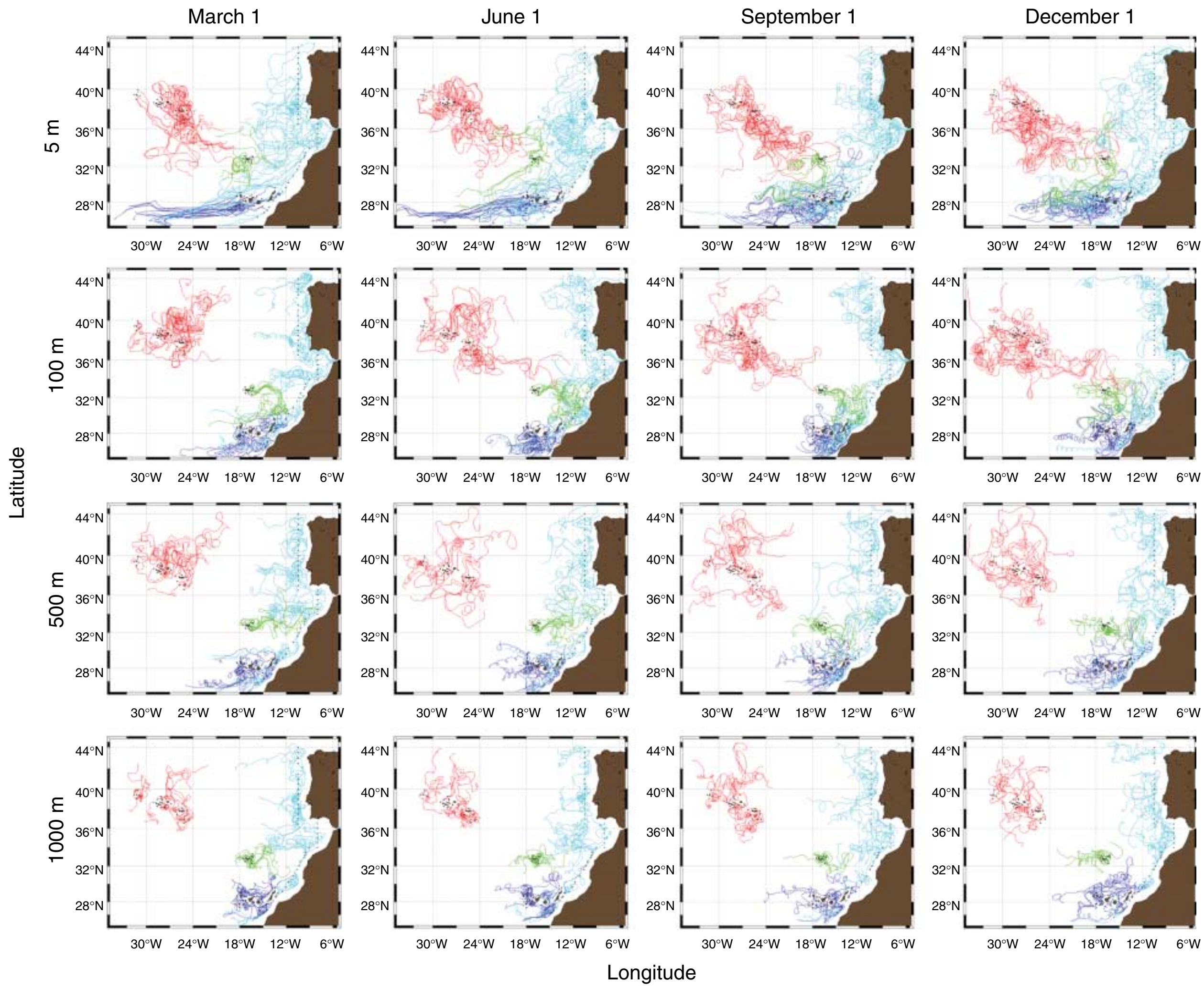

Fig. 6 Seasonal variability study. These simulations were performed releasing particles on March, June, September, and December of year 1, around the different release/source areas (AZ, Azores Archipelago; MA, Madeira Archipelago; CA, Canary Archipelago; IP, Iberian Peninsula; GI, Strait of Gibraltar; and NWA, Northwest Africa) and at different constant depths (5, 100, 500, and 1000 m). (Black dots mark the release position of the particles; red lines represent the trajectories of the particles released at the AZ; green lines are the trajectories of particles released at the MA; blue lines are the trajectories of the particles released at the CA; light blue lines are the trajectories of particles released along the IP and African coasts, and along the GI).

following the westward propagation of the CaC (Fig. 9A). The particles released at the IP coast traveled southward, probably due to the PoC, which joins the NAC with the AzC and CaC. However, particles released northerly in the IP traveled eastward toward the Cantabrian Sea (Fig. 9B), probably due to the Navidad Current (NaC; Pingree and Le Cann 1990), a branch of the Poleward Current that enters the Cantabrian Sea. For particles released in the AZ, MA, and IP, the principal sink was the WB, with a high percentage of particles reaching this limit (99.90%, 99.40%, and 72.48%, respectively; Table 3A). The fastest particles took 553, 360, and 592 d, respectively, to reach the WB limit. The particles released at GI and NWA were directly linked with the CaC southward drift (Fig. 9B). The fastest particle released at GI reached CA in 176 d, but a particle released at NWA can reach CA in <1 d (Table 4A). For CA and NWA coast sources, the principal sink was the SB, with 99.80% and 91.70% of the particles crossing this boundary. The fastest particles took 17 d to travel from CA to SB, and <1 d from NWA (Table 4A). Almost half (45.99%) of the particles released at GI crossed the NWA limits, and a similar proportion (46.72%) crossed the SB (Table 3A), with a travel time of 86 and 199 d, respectively (Table 4A).

© 2013 by the Association for the Sciences of Limnology and Oceanography, Inc. / e-ISSN 2157-3689

ASLO Association for the Sciences of Limnology and Oceanography
DUKE UNIVERSITY PRESS

Downloaded by guest on May 26, 2013

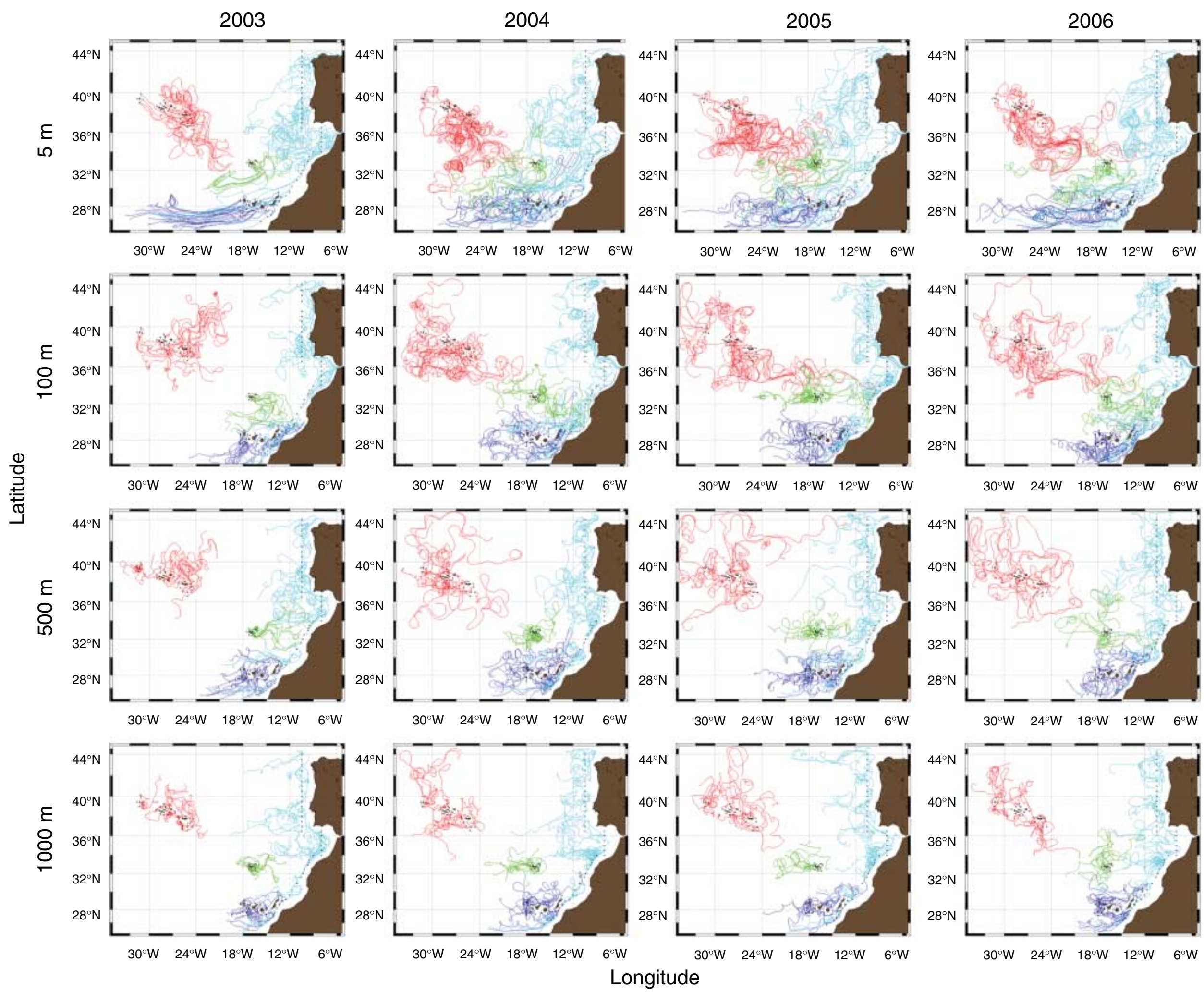

Fig. 7 Interannual variability study. These simulations were performed releasing particles on January 1 of each four years of the Regional Oceanic Modeling System (ROMS), around the different release/source areas (AZ, Azores Archipelago; MA, Madeira Archipelago; CA, Canary Archipelago; IP, Iberian Peninsula; GI, Strait of Gibraltar; and NWA, Northwest Africa) and at different constant depths (5, 100, 500, and 1000 m). (Black dots: initial position of the particles; red lines represent the trajectories of the particles released at the AZ; green lines the trajectories of the particles released at the MA; blue lines the trajectories of the particles released at the CA; light blue lines are the trajectories of the particles released along the IP, African coasts, and GI).

Particles released between 20 and 200 m

[13] The influence of the AzC was prominent at this depth range. The particles released in the AZ traveled eastward to the IP (51.50%) and subsequently to the GI, eventually reaching the Gulf of Cádiz (65.47%; Fig. 10A; Table 3B). The fastest particle reached the IP and the GI in 808 and 673 d, respectively (Table 4B). Some particles reached the NWA coast (34.43%) following the CaC direction (Fig. 10A) in 578 d (Table 4B). Only 1.90% of particles reached MA; the fastest particle took 581 d (Table 4B). From MA, the particles drifted southward to the CA (73.15%; Table 3B); the fastest particle did so in 262 d (Table 4B). Once in the CA, particles traveled southwest (Fig. 10A), with a high percentage of them crossing the SB (86.64%). Particles released along the continental shelf were transported parallel to the coast (Fig. 10B). About half (47.42%) of the particles released along IP crossed the limit of GI, the fastest in < 1 d (Tables 3B, 4B). The NaC influenced the particles released at the north of the IP, and 57.66% of the particles released at the GI reached the IP. Among particles released at the NWA coast, 25.55% reached the CA, following the CaC, and 37.34% crossed the SB (Table 3B). The fastest particles took < 1 d to reach both CA and the SB (Table 4B).

© 2013 by the Association for the Sciences of Limnology and Oceanography, Inc. / e-ISSN 2157-3689

Downloaded by guest on May 26, 2013

Table 3 Physical connectivity between source (rows) and sink (columns) regions (measured as percentage of particles reaching sink areas). Boldface numbers indicate the largest percentages of particles reaching the different destinations. AZ, Azores Archipelago; MA, Madeira Archipelago; CA, Canary Archipelago; IP, Iberian Peninsula; GI, Strait of Gibraltar; NWA, Northwest Africa; NB, North Boundary; SB, South Boundary; WB, West Boundary.

Depth	AZ	MA	CA	IP	GI	NWA	NB	SB	WB
A — 1–10 m									
AZ	–	36.83	7.09	0	0	0	0	59.48	**99.90**
MA	0	–	23.35	0	0.10	0.10	0	83.83	**99.40**
CA	0	0	–	0	0	15.72	0	**99.80**	66.99
IP	0	5.90	42.75	–	31.20	22.60	17.94	54.55	**72.48**
GI	0	0	35.04	40.15	–	45.99	0	**46.72**	47.45
NWA	0	0	67.90	0	0	–	0	**91.70**	63.97
B — 20–200 m									
AZ	–	1.90	7.39	51.50	**65.47**	34.43	27.84	6.69	0
MA	0	–	73.15	0.40	0.80	29.14	0	**95.71**	0
CA	0	0	–	0	0	66.90	0	**86.64**	0
IP	0	0	0	–	**47.42**	0.74	31.20	0	0
GI	0	0	0	**57.66**	–	3.65	0	0	0
NWA	0	0	25.55	6.11	15.28	–	0	**37.34**	0
C — 300–500 m									
AZ	–	4.49	4.19	18.06	7.29	8.38	**71.56**	4.59	1.20
MA	1.50	–	58.78	27.64	26.75	**73.55**	2.40	61.18	4.49
CA	0	0	–	0	0	47.25	0	**95.68**	2.95
IP	12.04	3.69	4.67	–	20.39	16.46	**45.70**	3.19	0
GI	2.92	1.46	4.38	**97.08**	–	12.41	4.38	3.65	0
NWA	0.66	0.22	52.18	10.92	13.32	–	0.66	**66.38**	3.06
D — 600–2000 m									
AZ	–	0.80	0.30	0.50	0.20	0.40	**42.51**	0.10	13.07
MA	6.79	–	8.98	18.96	29.64	**55.49**	2.99	2.10	0.30
CA	0.39	0.20	–	1.38	4.13	53.34	0.10	**53.93**	13.85
IP	13.27	4.18	0.74	–	7.62	3.19	**29.24**	0	1.47
GI	13.14	7.30	0.73	**57.66**	–	13.14	10.95	0	0.73
NWA	3.06	1.97	21.40	8.52	13.54	–	1.72	**45.41**	7.64

Intermediate water route, 300–500 m

[14] Particles released from the AZ at this depth range traveled mainly to the north and northeast (Fig. 11A); 71.56% of the particles crossed the NB, with a travel time of 217 d for the fastest particle (Tables 3C, 4C). The influence of the AzC is weak at these depths; thus, only 18.06% of the particles released in the AZ reached the IP, and 7.29% reached the GI and the Gulf of Cádiz (Fig. 11A; Table 3C), in 707 and 959 d respectively (Table 4C). Moreover, only 4.49% and 4.19% of the particles reached the MA and the CA sinks, respectively, in 657 d and 1138 d (Table 4C). Most particles released in the MA traveled eastward following two different branches: one to the north, reaching the GI (26.75%) and the IP (27.64%); and one traveling south, where 73.55% the particles reached the NWA coast. The fastest particle took 286 d to cross the GI limit, 339 d to cross the IP limit, and 212 d to cross the NWA limit (Table 4C). Of the particles released at CA, 95.68% reached the SB after 26 d considering a southwest drift induced by the CaC (Fig. 11A; Tables 3C, 4C). Particles released along continental shelf were transported parallel to the coast (Fig. 11B). The effect of the NaC, traveling toward the Cantabria Sea, was also evident. Remarkably, 97.08% of particles released at GI reached the IP coast in <1 d (Table 4C).

Deep-water routes, 600–2000 m

[15] The mean transport pathway from the AZ was northward, although only 42.51% of the particles crossed the NB (Fig. 12A; Table 3D) in as little as 322 d (Table 4D). Few particle trajectories traveled

© 2013 by the Association for the Sciences of Limnology and Oceanography, Inc. / e-ISSN 2157-3689

Downloaded by guest on May 26, 2013

Table 4 Travel time (d) for the fastest particle between source (rows) and sink (columns) regions. AZ, Azores Archipelago; MA, Madeira Archipelago; CA, Canary Archipelago; IP, Iberian Peninsula; GI, Strait of Gibraltar; NWA, Northwest Africa; NB, North Boundary; SB, South Boundary; WB, West Boundary.

Depth	AZ	MA	CA	IP	GI	NWA	NB	SB	WB
A — 1–10 m									
AZ	–	332	767	–	–	–	–	662	553
MA	–	–	101	–	470	359	–	201	360
CA	–	–	–	–	–	0	–	17	255
IP	–	245	310	–	0	88	0	491	592
GI	–	–	176	1	–	86	–	199	574
NWA	–	–	0	–	–	–	–	0	433
B — 20–200 m									
AZ	–	581	747	808	673	578	222	829	–
MA	–	–	262	444	401	220	–	346	–
CA	–	–	–	–	–	0	–	18	–
IP	–	–	–	–	0	1685	0	–	–
GI	–	–	–	1	–	145	–	–	–
NWA	–	–	0	244	78	–	–	0	–
C — 300–500 m									
AZ	–	657	1138	707	959	907	217	1241	606
MA	1410	–	330	339	286	212	991	433	1371
CA	–	–	–	–	–	0	–	26	992
IP	824	1460	2185	–	0	465	0	2478	–
GI	1029	1290	1964	1	–	615	1083	2338	–
NWA	1345	2116	0	242	79	–	1951	0	1047
D — 600–2000 m									
AZ	–	1760	3273	2373	2587	2463	322	3456	715
MA	1176	–	579	848	704	430	1808	1235	2851
CA	3184	2899	–	1090	677	0	3172	16	1736
IP	828	1183	2445	–	0	564	0	–	3352
GI	1039	866	3188	1	–	541	2131	–	2626
NWA	1360	1965	0	344	64	–	2413	0	2173

southward, and $<1\%$ reached MA and CA in 1760 d and 3273 d, respectively (Table 4D). The influence of the AzC was not seen at these depths. Particles released in the MA traveled to the east following two different branches, as in the 300–500 m range (Fig. 12A). The north branch reached the GI and the IP (29.64% and 18.96%, respectively; Table 3D) in 704 and 848 d, respectively. A few particles traveled to the AZ (6.79%) in 1176 d (Table 4D). The south branch, with 55.49% of the particles crossing the NWA limit, followed the CaC, joining their trajectories with particles released at the CA (Fig. 12A; Table 3D). It took 579 d for the fastest particle to travel from MA to CA (Table 4D). The particles released along the IP coast traveled northwest; 13.27% of them reached the AZ, and 29.24% crossed the NB (Fig. 12B; Table 3D), in 828 d and <1 d, respectively (Table 4D). More than half (57.66%) of the particles released along the GI reached the IP, mainly the south part, in 1 d (Tables 3D, 4D). A small portion of the particles reached the AZ (13.14%) and the NB (10.95%) in 1039 and 2131 d, respectively (Table 4D). These particles followed the northwest trajectory of the MWO, concurrent with the pathways observed by Defant (1956), Richardson and Mooney (1975), and Sy (1988).

Mediterranean Intermediate Water (800–1200 m)

[16] We undertook a study of the transport influenced by the MWO at this depth. We released particles at 800 m (upper core) and at 1200 m (lower core), as has been proposed in other studies (e.g., Ambar and Howe 1979a, 1979b; Borenäs et al. 2002). The particles were released at 8° W, where the MIW is thought to reach an equilibrium level below the NACW because of its density.

© 2013 by the Association for the Sciences of Limnology and Oceanography, Inc. / e-ISSN 2157-3689

Downloaded by guest on May 26, 2013

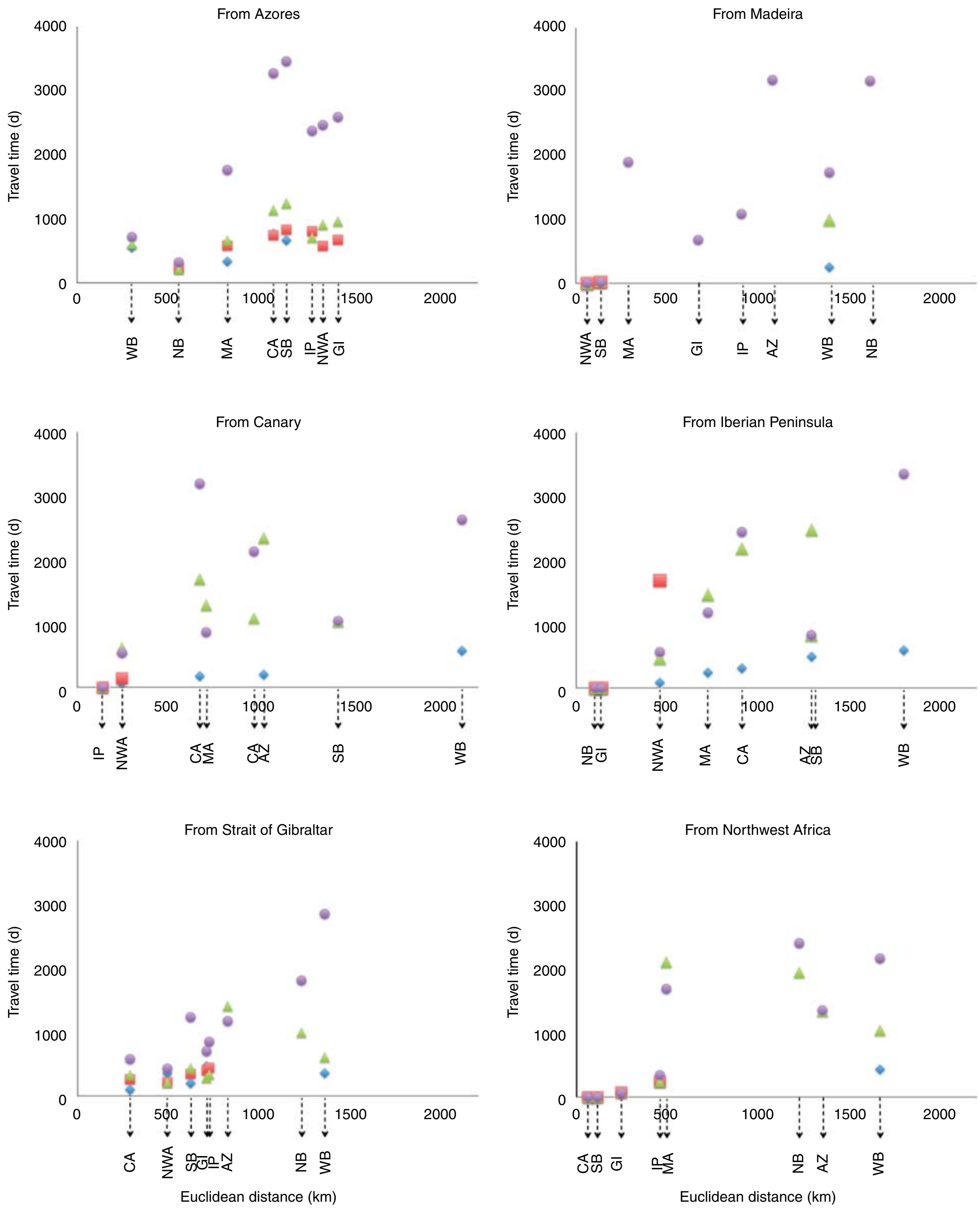

Fig. 8 Relationship between travel time (d) for the fastest particle in its journey and the Euclidean distance (km) between source and sink areas. Arrows on the x-axis indicate the approximate location of each site. enabling the measure of the relative distance between them. Depth layers are represented with different symbols: blue diamonds, 1 – 10 m; red squares, 20 – 200 m; green triangles, 300 – 500 m; purple circles, 600 – 2000 m. AZ, Azores Archipelago; MA, Madeira Archipelago; CA, Canary Archipelago; IP, Iberian Peninsula; GI, Strait of Gibraltar; NWA, Northwest Africa; NB, North Boundary; SB, South Boundary; WB, West Boundary.

© 2013 by the Association for the Sciences of Limnology and Oceanography, Inc. / e-ISSN 2157-3689

Downloaded by guest on May 26, 2013

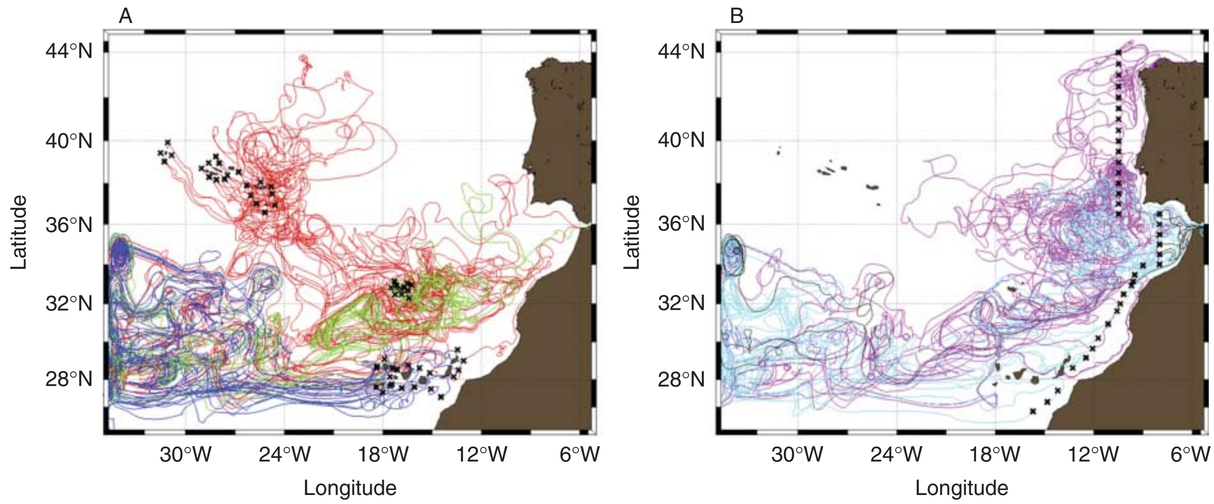

Fig. 9 Lagrangian pathways of particles released at the surface (1 – 10 m). A — Particles released from the Macaronesian archipelagos. B — Particles released along the continental boundaries and from the Strait of Gibraltar. Black crosses represent the release location; circles represent the end location. Lines represent trajectories of the particles: red, those released around the Azores Archipelago; green, around the Madeira Archipelago; blue, around the Canary Archipelago; pink, along Iberian Peninsula coast; black, along the Strait of Gibraltar; light blue, along the African coast.

Particles were transported westward, turning northward near Cape St. Vicente, at the southwestern corner of the IP. An aggregation of particles near the Estremadura Promontory (location noted in Fig. 1) is evident in Fig. 13A. A fraction of the particles entered the interior of the North Atlantic moving northwest. These results are consistent with the MIW pathways observed with RAFOS floats (i.e., deep Lagrangian drifters; e.g., Baringer and Price 1997; Bower et al. 2002).

Discussion

[17] To the best of our knowledge, this is the first study to characterize the transport pathways in the NEA, particularly in the Canary Basin. It is difficult to validate the current calculations because it is difficult to carry out Lagrangian drifting studies in such a large basin when using different sources and destination sites and different depths. Global drifter programs such as the one carried out by GOOS (Global Ocean Observing System)

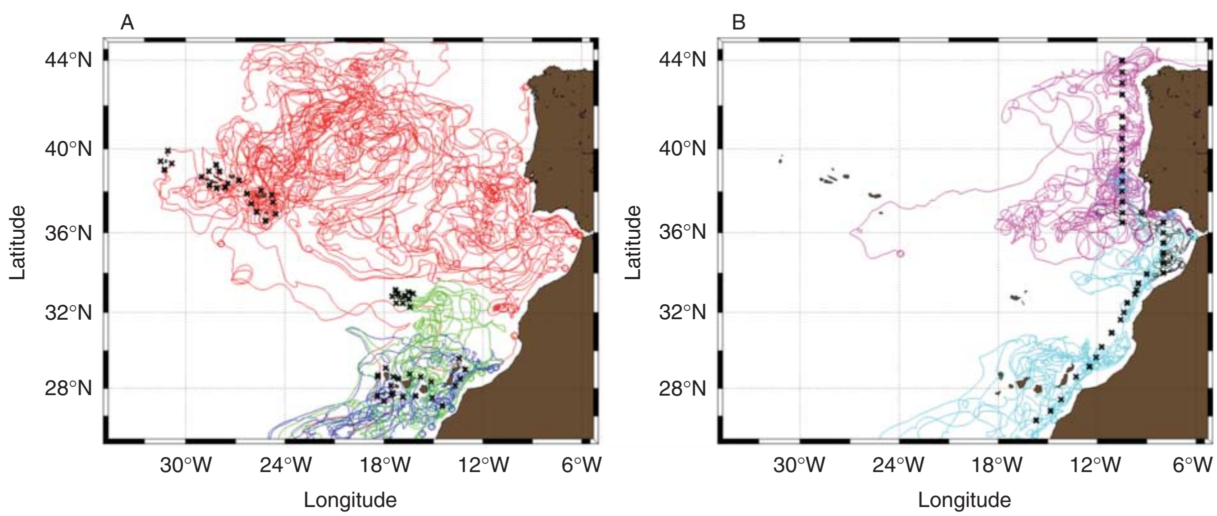

Fig. 10 Lagrangian pathways released between 20 and 200 m. A — Particles released from the Macaronesian archipelagos. B — Particles released along the continental boundaries and from the Strait of Gibraltar. Lines and symbols are as in Fig. 9.

© 2013 by the Association for the Sciences of Limnology and Oceanography, Inc. / e-ISSN 2157-3689

Downloaded by guest on May 26, 2013

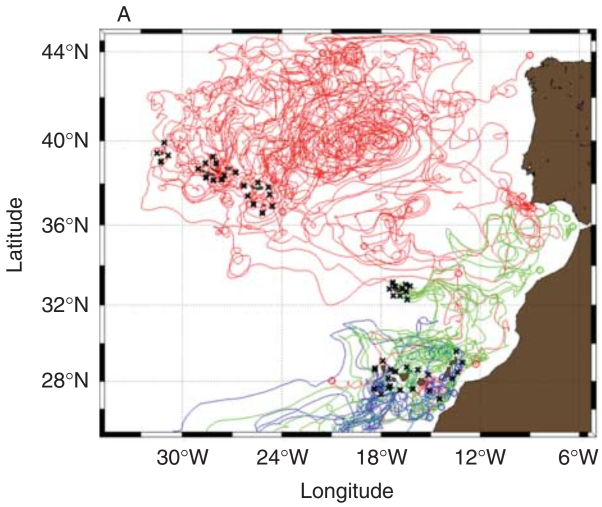

Fig. 11 Lagrangian pathways released between 300 and 500 m. A — Particles released from the Macaronesian archipelagos. B — Particles released along the continental boundaries and from the Strait of Gibraltar. Lines and symbols are as in Fig. 9.

only consider the use of SVP (Surface Velocity Program) drifters, which are transported by surface currents. In other global ocean-observing programs using Argo and/or RAFOS, the buoys are active profilers subjected to transport by different water masses at different times. As in other case studies, numerical models can be used as an appropriate tool to characterize some of the general routes. However, results from biological and chemical distributions can be used to support some of our findings, recognizing that not all the transport pathways were mapped, nor did all organisms and chemicals follow similar trajectories. In this context, we hope to stimulate further theoretical discussions, as well as more Lagrangian observations in the region. Future studies should help to clarify issues such as the "self-seeding" processes occurring around the islands and continental shelves, taking into account the coastal dynamics and the effect of returning particles crossing the boundaries, all of which can lead to an under- and overestimation of population connectivity.

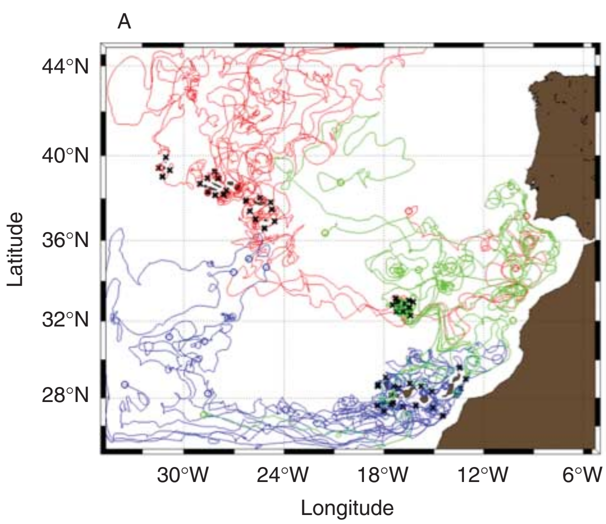

Fig. 12 Lagrangian pathways released between 600 and 2000 m. A — Particles released from the Macaronesian archipelagos. B — Particles released along the continental boundaries and from the Strait of Gibraltar. Lines and symbols are as in Fig. 9.

© 2013 by the Association for the Sciences of Limnology and Oceanography, Inc. / e-ISSN 2157-3689

Downloaded by guest on May 26, 2013

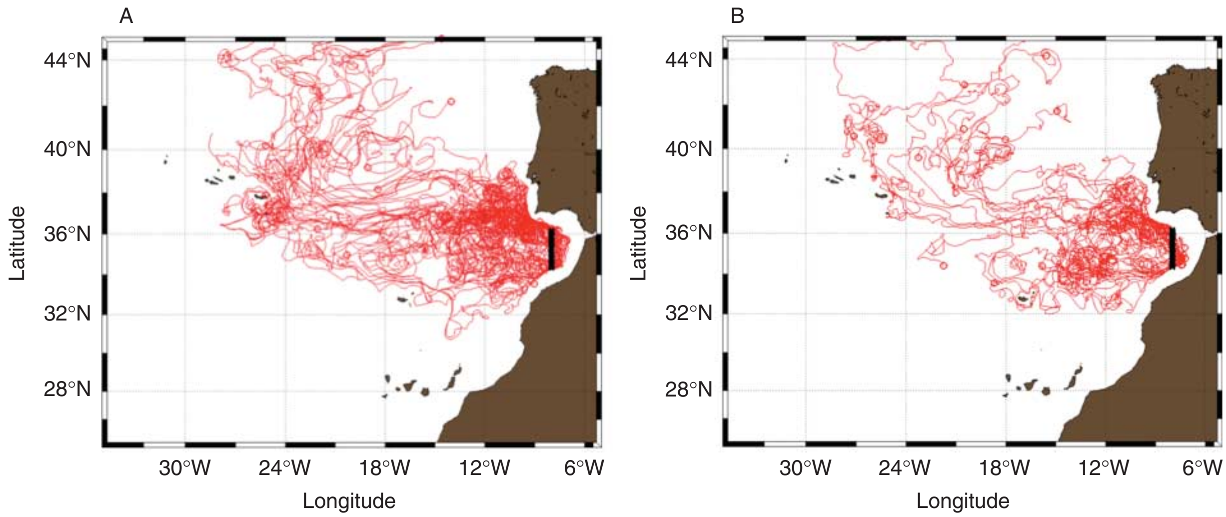

Fig. 13 Study of the Mediterranean Intermediate Water, considering the two main cores: 800 m depth (A; upper core) and 1200 m depth (B; lower core). Particles were released at 8° W, where the MIW reaches equilibrium. Black crosses represent the initial position, and the circles the end of the trajectories, terminated inside the domain.

Links to Biological Studies

[18] Ocean currents have a strong influence on the dynamics of many marine species (e.g., Roughgarden et al. 1988; Gaylord and Gaines 2000). Most marine species have a larval stage that is transported in the plankton, leading to the potential of dispersal over broad geographic regions (Thorson 1950; Strathmann 1985). This pelagic phase, with a duration ranging from days to months, plays a key role in the interconnection of marine metapopulations (Botsford et al. 2003), especially in species with relatively sessile adults. Marine species with a long larval phase are expected to achieve high levels of dispersal, resulting in panmixia (i.e., lack of genetic differentiation over large scales). However, there are species with lecithotrophic (yolk) larvae (spending limited time in the plankton before settling) and others that are direct developers (no larval stage) that have geographic distributions comparable to those with a pelagic stage. Some of the ways in which these organisms can expand their distributions are drifting, rafting, hitchhiking, creeping, and hopping (Winston 2012). Buoyant materials, such as logs, plastics, and so forth, can also transport marine and terrestrial organisms over oceanic scales.

Sponge: Phorbas fictitius *(Bowerbank 1866)*

[19] Whereas the adult phase of this species is sessile, its lecithotrophic larvae are planktonic for a few days to 2 weeks, which allows for the dispersion of this sponge species (Maldonado 2006). *Phorbas fictitius* has a wide distribution range in the NEA (from the west coast of Scotland to the CA) and Mediterranean (from Alborán to the Aegean Sea). Xavier et al. (2010) examined the genetic structure and phylogeographical history of this species, based on mitochondrial DNA sequences of cytochrome c oxidase. They found a high genetic structure consistent with the low dispersal potential, but there was a nonsignificant differentiation between the AZ and CA populations (separated by 1500 km). This suggested occasional long-distance dispersal events, most likely due to the drift of small fragments containing embryos (Xavier et al. 2010). This is consistent with the observation of Maldonado and Uriz (1999) that small fragments of reproductive sponges, containing embryos, broken by wave or predatory action can be transported by currents and recruited to new areas, thus facilitating long-range dispersion of this species. In their opinion, island-to-mainland dispersal is more likely given the eastward-flowing currents characteristic

© 2013 by the Association for the Sciences of Limnology and Oceanography, Inc. / e-ISSN 2157-3689

Downloaded by guest on May 26, 2013

of this region, such as the AzC and the NAC (Reverdin et al. 2003). This nonsignificant differentiation between AZ and CA *P. fictitius* populations is consistent with our surface and intermediate routes (1–500 m). Figs. 9–11 show how particles released at the AZ, between depths of 1 and 500 m, reached the CA due to the AzC on a timescale of 24 months.

Achelata lobsters: Scyllarides latus *(Latreille 1803) and* Palinurus elephas *(Fabricius 1787)*

[20] Both Scyllaridae and Palinuridae families have long larval phases, lasting up to 24 months in some species (Phillips and Sastry 1980; Booth et al. 2005). Froufe et al. (2011) tested two competing phylogeographic hypotheses by using lobster species sampled in this region: panmixia due to long-distance dispersion and population structuring due to environmental factors (e.g., oceanographic barriers and currents). They found that there was panmixia in *S. latus* and *P. elephas* in the Macaronesian archipelagos and across the NEA. The surface routes identified in our study may explain the panmixia in Macaronesian islands, via the AzC and CaC, which allow connectivity among islands (Figs. 7, 8). Moreover, our travel times for particles between the Macaronesian islands of <24 months lie within the larval stage of these species (Table 4).

Fishes: Sardina pilchardus *(Walbaum 1792) and* Engraulis encrasicolus *(Linnaeus 1758)*

[21] The southwest eddy corridor generated by the interaction of the CaC with the CA (Barton et al. 2004; Sangrà et al. 2009) also interacts with upwelling filaments, favoring connection between the continental African coast and the CA. As a result of these upwelling filaments, a well-known corridor of egg and larval transport is formed between the African neritic zone and the CA (Rodríguez et al. 1999). This offshore arrival of small pelagic larvae has a positive impact on the CA fisheries (Bécognée et al. 2006). Sardine (*Sardina pilchardus*) and anchovy (*Engraulis encrasicolus*) are both present in the offshore transport (Brochier et al. 2008, 2011). Brochier et al. (2011) used an ichthyoplankton transport model (Ichthyop) forced by ROMS solutions to identify the mechanism by which sardine and anchovy larvae are transported to Gran Canaria Island from the African continental shelf. Their study focused on the CA subregion of the NEA, but the results were coherent with the field observation of egg distribution. The connectivity pathway between the African coast and the CA are also supported by our qualitative results, particularly in the top layers (1 – 200 m; Figs. 7, 8). Furthermore, according to our calculations, the fastest particle takes <1 d to travel from the NWA coast to the CA, which is compatible with the duration of fish larval stage (Table 4).

Fish: Conger conger *(Linnaeus 1758)*

[22] The European conger eel (*Conger conger*) is a deep-water marine fish widely distributed along shores of NEA, the Mediterranean Sea, and the western Black Sea (Bauchot and Saldanha 1986). The leptocephalic (flat and transparent) larval stage can persist up to 2 y in pelagic environments (Correia et al. 2006), allowing the large-scale dispersion of the species. Correia et al. (2012) applied both molecular and otolith-based analyses to provide new information on the population structure and connectivity of the European conger eel across the northeastern Atlantic and western Mediterranean (i.e., Ireland, north and south of Portugal, AZ, MA, and Mallorca). Their results support the hypothesis of a broad-scale dispersal of conger eel larvae, with limited connectivity between juvenile fish populations at large spatial scales. A previous study (Correia et al. 2011) of the oxygen and carbon isotopic signatures in the otoliths of *C. conger* suggests a low level of connectivity between NEA and Mediterranean fishery areas. Small young larvae were captured near the AZ, indicating a spawning area in the Mid-Atlantic Region (Correia et al. 2002, 2003). Our surface and intermediate transport pathways (1–500 m; Figs. 9–11) can explain these results. The larvae spawning near the AZ could drift eastward, reaching the Portuguese coast and the MA via the AzC, which would take <2 y based on our travel time estimates (Table 4). We also observed a northward transport that could explain the connection between the AZ and Ireland (northern boundary), despite the fact that our ROMS domain does not extend as far north as Ireland.

© 2013 by the Association for the Sciences of Limnology and Oceanography, Inc. / e-ISSN 2157-3689

Downloaded by guest on May 26, 2013

A Chemical Example: Prestige *Oil Tanker Accident*

[23] On 19 November 2002, the *Prestige* oil tanker accident resulted in the spill of 60,000 tons of heavy fuel off the north coast of Galicia (northwestern Spain; Carracedo et al. 2006). Wind drove this fuel toward the Galician coast in several coastal locations. In addition, multiple oil slicks were pushed by the wind along the Cantabrian and French Atlantic coasts during the following months. Garcia-Soto (2004) analyzed the eastward trajectory of oil slicks along the coast of northern Spain, using combined airborne observations, thermal infrared, altimeter, and *Envisat* ASAR (Advanced Synthetic Aperture Radar) satellite measurements. AVHRR images showed the entrance of the Poleward Current (e.g., Pingree and Le Cann 1989, 1990) in the Bay of Biscay around Galicia, extending eastward along the Cantabrian shelf and slopes. Supplementary altimeter data confirmed a continuous extension of the current from Galicia to the vicinity of Bilbao. The distribution of oil slicks in the *Envisat* ASAR image of 16 December appears to trace the NaC coming from the west (see Fig. 1 for NaC approximate location). The trajectory followed by the oil spill (Garcia-Soto 2004, figure 1) is consistent with our results, whereby the NaC together with the wind might be responsible for the spread of the oil along the Cantabrian and French Atlantic coasts.

[24] Several attempts were made to forecast the drift, spreading, and stranding of the *Prestige* oil spill during and after the crisis (e.g., Montero et al. 2003; Daniel et al. 2004), leading to the development of models to predict oil and chemical spill trajectories (e.g., Jordi et al. 2006; Sotillo et al. 2008; Periáñez and Caravaca 2010). The present study suggests important pathways to consider in the event of future oil spills in the NEA.

[25] The AzC was well depicted by the particles released around the AZ. The signal was observed in the first 500 m of depth, although its influence is stronger in the top layers. As described in the literature, particles influenced by the AzC mostly traveled eastward, reaching the Gulf of Cádiz (e.g., Martins et al. 2002). Meanwhile, an eastward branch of the AzC flows north and off around Madeira Island, joining the CaC, which originates between the MA and the African coast (Stramma 1984). Lagrangian pathways between 20 and 500 m of depth confirmed that the CaC moves southwestward through the CA, parallel to the African coast. We also observed the PoC, a southward current followed by the particles released at the IP at the surface. At the north of the IP, between 1 and 500 m, the NaC (Pingree and Le Cann 1992) was observed, consisting in the intrusion of particles following the Iberian Poleward current in the Cantabrian Sea. Between 600 and 2000 m, the strong influence of the MIW in the transport of the particles was observed. A focused study of the MWO region shows that our results are consistent with the MIW pathways described in other studies (e.g., Baringer and Price 1997; Bower et al. 2002): a westward transport turning northward around Cape St. Vicente, with a large accumulation of particles on the southwest coast of the IP, and a northward intrusion of particles in interior of the North Atlantic.

[26] Because the ocean currents play an important role in the distribution of many marine species, their geographical distribution will be linked with the currents' flow. The connectivity of sardine (*Sardina pilchardus*) and anchovy (*Engraulis encrasicolus*) between the African coast and the CA, due to the upwelling filaments generated by the CaC, is possible due to the proximity of the islands to the mainland, considering that the pelagic phase of these species lasts only 30 d. However, marine species with long larval phases are expected to reach high levels of dispersal, resulting in panmixia. We found reports of three species, which support this finding: two species of Achelata lobsters, *Scyllarides latus* and *Palinurus elephas*, and one fish species, *Conger conger*. These species have long larval phases (24 months) and thus a possibility of having a wide distribution in the NEA (IP coast and Macaronesian islands). The Macaronesian islands, the IP, and the African coast are connected due to the influence of the AzC and CaC. The sponge *Phorbas fictitius* also supports the existence of the connectivity between AZ and the CA, because of the drift of small fragments of reproductive sponges (Maldonado and Uriz 1999), resulting in little differentiation between populations separated by at least 1500 km. Finally, the path followed by the oil spilled from the *Prestige* accident is directly related to climatic and oceanographic conditions that we found to dominate at and following the accident. The presence of southwesterly winds and the entrance of warm water

© 2013 by the Association for the Sciences of Limnology and Oceanography, Inc. / e-ISSN 2157-3689

Downloaded by guest on May 26, 2013

brought by the NaC to the Bay of Biscay during the months after the accident were responsible for the dispersion over the Galician, Cantabrian, French, and Atlantic coasts.

Significance to Aquatic Environments

[27] The ability to track the movements of oceanic currents spatially is critical to our understanding of the direction and timing of biological and chemical processes. This is especially important in areas like the NEA region, where complex bathymetry, topography, and inflows from the Mediterranean Sea make it difficult to study currents empirically. Consequently, our approach using numerical modeling has provided important information on the Lagrangian trajectories of particles carried by these currents. Importantly, we note that the trajectories vary with depth, and these patterns are important for transporting scalar quantities.

[28] Lagrangian transport pathways are important for fisheries management, conservation biology, mitigating pollution events, and rescue missions, among others. Despite being a general approach, this study provides a map of the main Lagrangian transport routes in the NEA and provides a perspective for subsequent basin-scale studies. For species of commercial interest and with long-lived larvae that can afford long-distance (open-ocean) dispersal, such as lobsters and eels, this approach may provide insight into larval and adult distributions. High spatial and temporal coastal resolution studies addressing larval connectivity issues, including daily migration, should be considered (e.g., Paris et al. 2005; Mitarai et al. 2009; Kool et al. 2011). Understanding the general routes of dispersion at a basin scale can also help define protected areas, that is, connection between sites (Fogarty and Botsford 2007), which most likely will cross several economic exclusive zones. In the transport of chemical elements, our study suggests important pathways to consider in future accidents, given the large volumes of both crude oil and refined products that are transported within this region. According to the International Tanker Owners Pollution Federation, over 5000 metric tons of oil was spilled in the NEA region from 1974 to 2003 (see http://www.itopf.com/). Empirical studies should focus on further validating these transport routes to adequately prepare management and response strategies for future pollution events.

Acknowledgments The authors thank Cheryl Harrison for commenting on earlier versions of the manuscript. This work was carried out in the scope of the INTERREG-IV project “0313_RAIA_1_E,” cofinanced by the POCTEP program within the European Union transnational initiative. Numerical model solutions were calculated at CIIMAR’s HPC unit, acquired by FCT pluriannual funds (PesT-C/MAR/LA0015/2011), and further expanded with funding from the RAIA.co project. Ariane work was partially carried out in a small computing unit from the Center for Mathematical Sciences (CCM) of the University of Madeira. CCM has also hosted interaction among some of the participating researchers. ROMS_AGRIF and ROMS_TOOLS were provided by the IRD team (http://www.romsagrif.org). Comments provided by Joe Ackerman and Hidekatsu Yamazaki and by two anonymous reviewers substantially improved subsequent versions of the manuscript.

References

Álvarez, I., et al. 2009. A winter upwelling event in the Northern Galician Rías: Frequency and oceanographic implications. Estuar. Coast. Shelf Sci. **82**: 573–582, doi:10.1016/j.ecss.2009.02.023.

Ambar, I., and M. R. Howe. 1979a. Observations of the Mediterranean outflow—I. Mixing in the Mediterranean outflow. Deep-Sea Res. A. **26**: 535–554, doi:10.1016/0198-0149(79)90095-5.

———, 1979b. Observations of the Mediterranean outflow—II. The deep circulation in the vicinity of the Gulf of Cadiz. Deep-Sea Res. A. **26**: 555–568, doi:10.1016/0198-0149(79)90096-7.

Baringer, M. O., and J. F. Price. 1997. Mixing and spreading of the Mediterranean outflow. J. Phys. Oceanogr. **27**: 1654–1677, doi:10.1175/1520-0485(1997)027<1654:MASOTM>2.0.CO;2.

Barton, E. D. 1998. Eastern boundary of the North Atlantic: Northwest Africa and Iberia coastal segment. The Sea. The Global Coastal Ocean: Regional Studies and Syntheses. P. 633–658. *In* A. R. Robinson and K. H. Brink [eds.], John Wiley & Sons.

Barton, E. D., J. Aristegui, P. Tett, and E. Navarro-Perez. 2004. Variability in the Canary Islands area of filament-eddy exchanges. Prog. Oceanogr. **62**: 71–94, doi:10.1016/j.pocean.2004.07.003.

Barton, E. D., P. Flament, H. Dodds, and E. G. Mitchelson-Jacob. 2001. Mesoscale structure viewed by SAR and AVHRR near the Canary Islands. Sci. Mar. **65**: 167–175.

Bauchot, M. L., and L. Saldanha. 1986. Fishes of the Northeastern Atlantic and the Mediterranean. UNESCO.

Bécognée, P., C. Almeida, A. Barrera, A. Hernández-Guerra, and S. Hernández-León. 2006. Annual cycle of clupeiform larvae around Gran Canaria Island, Canary Islands. Fish. Oceanogr. **15**: 293–300, doi:10.1111/j.1365-2419.2005.00390.x.

© 2013 by the Association for the Sciences of Limnology and Oceanography, Inc. / e-ISSN 2157-3689

Downloaded by guest on May 26, 2013

Blanke, B., M. Arhan, G. Madec, and S. Roche. 1999. Warm water paths in the equatorial Atlantic as diagnosed with a general circulation model. J. Geophys. Res. **29**: 2753–2768.

Blanke, B., and S. Raynaud. 1997. Kinematics of the Pacific Equatorial Undercurrent: An Eulerian and Lagrangian approach from GCM results. J. Phys. Oceanogr. **27**: 1038–1053, doi:10.1175/1520-0485(1997)027<1038:KOTPEU>2.0.CO;2.

Blanke, B., S. Speich, G. Madec, and K. Döös. 2001. A global diagnostic of interocean mass transfers. J. Geophys. Res. **31**: 1623–1632.

Bonhommeau, S., B. Blanke, A. M. Tréguier, N. Grima, E. Rivot, Y. Vermard, E. Greiner, and O. Le Pape. 2009. How fast can the European eel (*Anguilla anguilla*) larvae cross the Atlantic Ocean? Fish. Oceanogr. **18**: 371–385, doi:10.1111/j.1365-2419.2009.00517.x.

Booth, J. D., W. R. Webber, H. Sekiguchi, and E. Coutures. 2005. Diverse larval recruitment strategies within the Scyllaridae. N. Z. J. Mar. Freshw. Res. **39** (3): 581–592.

Borenäs, K., A. Wahlin, I. Ambar, and N. Serra. 2002. The Mediterranean outflow splitting—a comparison between theoretical models and CANIGO data. Deep Sea Res. Part II Top. Stud. Oceanogr. **49**: 4195–4205, doi:10.1016/S0967-0645(02)00150-9.

Borges, P. A. V., and V. K. Brown. 1999. Effect of island geological age on the arthropod species richness of Azorean pastures. Biol. J. Linn. Soc. Lond. **66**: 373–410, doi:10.1111/j.1095-8312.1999.tb01897.x.

Botsford, L. W., F. Micheli, and A. Hastings. 2003. Principles for the design of marine reserves. Ecol. Appl. **13** (suppl.): 25–31, doi:10.1890/1051-0761(2003)013[0025:PFTDOM]2.0.CO;2.

Bower, A., N. Serra, and I. Ambar. 2002. Structure of the Mediterranean Undercurrent and Mediterranean Water spreading around the south-western Iberian Peninsula. J. Geophys. Res. **107** (C10): 25-1–25-19, doi:10.1029/2001JC001007.

Briggs, J. C. 1970. A faunal history of the North Atlantic Ocean. Syst. Zool. **19**: 19–34, doi:10.2307/2412025.

Brochier, T., C. Lett, J. Tam, P. Fréon, F. Colas, and P. Ayón. 2008. An individual-based model study of anchovy early life history in the northern Humboldt Current system. Prog. Oceanogr. **79**: 313–325, doi:10.1016/j.pocean.2008.10.004.

Brochier, T., et al. 2011. Ichthyoplankton transport from the African coast to the Canary Islands. J. Mar. Syst. **87**: 109–122, doi:10.1016/j.jmarsys.2011.02.025.

Carracedo, P., S. Torres-López, M. Barreiro, P. Montero, C. F. Balseiro, E. Penabad, P. C. Leitao, and V. Pérez-Muñuzuri. 2006. Improvement of pollutant drift forecast system applied to the *Prestige* oil spills in Galicia Coast (NW of Spain): Development of an operational system. Mar. Pollut. Bull. **53**: 350–360, doi:10.1016/j.marpolbul.2005.11.014.

Correia, A. T., C. Antunes, E. J. Isidro, and J. Coimbra. 2003. Changes in otolith microstructure and microchemistry during the larval development of the European conger eel (*Conger conger*). Mar. Biol. **142**: 777–789.

Correia, A. T., C. Antunes, J. M. Wilson, and J. Coimbra. 2006. An evaluation of the otolith characteristics of *Conger conger* during metamorphosis. J. Fish Biol. **68**: 99–119, doi:10.1111/j.0022-1112.2006.00881.x.

Correia, A. T., F. Barros, and A. Sial. 2011. Stock discrimination of European conger eel (*Conger conger* L.) using otolith stable isotope ratios. Fish. Res. **108**: 88–94, doi:10.1016/j.fishres.2010.12.002.

Correia, A. T., E. J. Isidro, C. Antunes, and J. Coimbra. 2002. Age, growth, distribution and ecological aspects of *Conger conger* leptocephali collected in the Azores, based on otolith analysis of premetamorphic specimens. Mar. Biol. **141**: 1141–1151, doi:10.1007/s00227-002-0908-4.

Correia, A. T., A. A. Ramos, F. Barros, G. Silva, P. Hamer, P. Morais, R. L. Cunha, and R. Castilho. 2012. Population structure and connectivity of the European conger eel (*Conger conger*) across the north-eastern Atlantic and western Mediterranean: Integrating molecular and otolith elemental approaches. Mar. Biol. **159**: 1509–1525, doi:10.1007/s00227-012-1936-3.

Cowen, R. K., and S. Sponaugle. 2009. Larval dispersal and marine population connectivity. Annu. Rev. Mar. Sci. **1**: 443–466, doi:10.1146/annurev.marine.010908.163757.

Daniel, P., P. Josse, P. Dandin, J. M. Lefevre, G. Lery, F. Cabioch, and V. Gouriou. 2004. Forecasting the *Prestige* oil spills, *In* Proceedings of the Interspill 2004 Conference, Trondheim, Norway. http://www.interspill.org/previous-events/2004/session1.php.

Da Silva, A. M., C. C. Young, and S. Levitus. Atlas of Surface Marine Data 1994.Vol. 1. Algorithms and Procedures, NOAA/NESDIS Tech. Rep. **6**. U.S. Department of Commerce.

Defant, A. 1956. Die Ausbreitung des Mittelmeerwassers im Nordatlantischen Ozean. Deep-Sea Res. **3** (suppl.): 465–470.

Dietrich, G., K. Kalle, W. Krauss, and G. Siedler. 1980. General Oceanography: An Introduction. John Wiley & Sons.

Dietrich, D. E., Y. H. Tseng, R. Medina, S. A. Piacsek, M. Liste, M. Olabarrieta, M. J. Bowman, and A. Mehra. 2008. Mediterranean Overflow Water (MOW) simulation using a coupled multiple-grid Mediterranean Sea/North Atlantic Ocean model. J. Geophys. Res. **113** (C7): C07027, doi:10.1029/2006JC003914.

Döös, K. 1995. Interocean exchange of water masses. J. Geophys. Res. **100** (C7): 13499–13514, doi:10.1029/95JC00337.

Durand, F., D. Shankar, F. Birol, and S. Shenoi. 2008. Estimating boundary currents from satellite altimetry: A case study for the east coast of India. J. Oceanogr. **64**: 831–845, doi:10.1007/s10872-008-0069-2.

Fernández, E., and R. D. Pingree. 1996. Coupling between physical and biological fields in the North Atlantic subtropical front southeast of the Azores. Deep-Sea Res. Part I Oceanogr. Res. Pap. **43**: 1369–1393.

Fogarty, M. J., and L. W. Botsford. 2007. Population connectivity and spatial management of marine fisheries. Oceanography (Wash. D.C.) **20**: 112–123, doi:10.5670/oceanog.2007.34.

© 2013 by the Association for the Sciences of Limnology and Oceanography, Inc. / e-ISSN 2157-3689

Downloaded by guest on May 26, 2013

Froufe, E., P. Cabezas, P. Alexandrino and M. Pérez-Losada. 2011. Comparative phylogeography of three lobster species from the Macaronesia (North East Atlantic). Phylogeography and Population Genetics in Crustacea. P. 157–173. *In* C. Held, S. Koenemann and C. D. Schubart [eds.], CRC Press, doi:10.1201/b11113-10.

Garcia-Soto, C. 2004. "Prestige" oil spill and Navidad flow. J. Mar. Biol. Assoc. U.K. **84**: 297–300, doi:10.1017/S002531540400918Xh.

Gaylord, B., and S. D. Gaines. 2000. Temperature or transport? Range limits in marine species mediated solely by flow. Am. Nat. **155**: 769–789, doi:10.1086/303357.

González, M., L. Ferrer, A. Uriarte, A. Urtizberea, and A. Caballero. 2008. Operational Oceanography System applied to the *Prestige* oil-spillage event. J. Mar. Syst. **72**: 178–188, doi:10.1016/j.jmarsys.2007.07.005.

Gould, W. J. 1985. Physical oceanography of the Azores Front. Prog. Oceanogr. **14**: 167–190, doi:10.1016/0079-6611(85)90010-2.

Hernández-Guerra, A., E. Fraile-Nuez, R. Borges, F. Lopez-Laatzen, P. Velez-Belchi, G. Parrilla, and T. J. Muller. 2003. Transport variability in the Lanzarote passage (eastern boundary current of the North Atlantic subtropical gyre). Deep Sea Res. Part I Oceanogr. Res. Pap. **50**: 189–200, doi:10.1016/S0967-0637(02)00163-2.

Hernández-Guerra, A., et al. 2002. Temporal variability of mass transport in the Canary Current. Canary Current. Deep-Sea Res. Part II Top. Stud. Oceanogr. **49**: 3415–3426, doi:10.1016/S0967-0645(02)00092-9.

Hernández-León, S., M. Gómez, and J. Arístegui. 2007. Mesozooplankton in the Canary Current system: The coastal-ocean transition zone. Prog. Oceanogr. **74**: 397–421, doi:10.1016/j.pocean.2007.04.010.

Izumo, T., J. Picaut, and B. Blanke. 2002. Tropical pathways, equatorial undercurrent variability and the 1998 La Niña. Geophys. Res. Lett. **29**: 37-1–37-4, doi:10.1029/2002GL015073.

Jordi, A., et al. 2006. Scientific management of Mediterranean coastal zone: A hybrid ocean forecasting system for oil spill and search and rescue operations. Mar. Pollut. Bull. **53**: 361–368, doi:10.1016/j.marpolbul.2005.10.008.

Käse, R. H., and G. Siedler. 1982. Meandering of the subtropical front south-east of the Azores. Nature **300**: 245–246, doi:10.1038/300245a0.

Käse, R. H., W. Zenk, T. B. Sanford, and W. Hiller. 1985. Currents, Fronts and Eddy Fluxes in the Canary Basin. Progr. Oceanogr. **14**: Pergamon.

Koch-Larrouy, A., R. Morrow, T. Penduff, and M. Juza. 2010. Origin and mechanism of Subantarctic Mode Water formation and transformation in the Southern Indian Ocean. Ocean Dyn. **60**: 563–583, doi:10.1007/s10236-010-0276-4.

Kool, J. T., C. B. Paris, P. H. Barber, and R. K. Cowen. 2011. Connectivity and the development of population genetic structure in Indo-West Pacific coral reef communities. Global Ecol. Biogeogr. **20** (5): 695–706.

Le Traon, P.-Y., and P. De Mey. 1994. The eddy field associated with the Azores Front east of the mid-Atlantic ridges as observed by the *Geosat* altimeter. J. Geophys. Res. **99** (C5): 9907–0023, doi:10.1029/93JC03513.

Machín, F., A. Hernández-Guerra, and J. L. Pelegrí. 2006. Mass fluxes in the Canary Basin. Prog. Oceanogr. **70**: 416–447, doi:10.1016/j.pocean.2006.03.019.

Maldonado, M. 2006. The ecology of sponge larvae. Can. J. Zool. **84**: 175–194, doi:10.1139/z05-177.

Maldonado, M., and M. J. Uriz. 1999. Sexual propagation by sponge fragments. Nature **398**: 476, doi:10.1038/19007.

Marchesiello, P., L. Debreu, and X. Couvelard. 2009. Spurious diapycnal mixing in terrain-following coordinate models: The problem and a solution. Ocean Model. **26**: 156–169, doi:10.1016/j.ocemod.2008.09.004.

Martins, C., M. Hamann, and A. Fiúza. 2002. Surface circulation in the eastern North Atlantic, from drifters and altimetry. J. Geophys. Res. **107** (C12): 3217, doi:10.1029/2000JC000345.

Mitarai, S., D. A. Siegel, J. R. Watson, C. Dong, and J. C. McWilliams. 2009. Quantifying connectivity in the coastal ocean with application to the Southern California Bight. J. Geophys. Res., C, Oceans. **114** (C10): C10026, doi:10.1029/2008JC005166.

Montero, P., et al. 2003. Oil spill monitoring, forecasting on the Prestige-Nassau accident. P. 1013–1029, *In* Proceedings 26th Artic, Marine Oil Spill Program (AMOP). Tech. Semin. **2**. Environment Canada.

New, A. L., Y. Jia, M. Coulibaly, and J. Dengg. 2001. On the role of the Azores Current in the ventilation of the North Atlantic Ocean. Prog. Oceanogr. **48**: 163–194, doi:10.1016/S0079-6611(01)00004-0.

Paris, C. B., R. K. Cowen, R. Claro, and K. C. Lindeman. 2005. Larval transport pathways from Cuban snapper (Lutjanidae) spawning aggregations based on biophysical modelling. Mar. Ecol. Prog. Ser. **296**: 93–106, doi:10.3354/meps296093.

Peliz, Á. J., J. Dubert, A. M. P. Santos, P. B. Oliveira, and B. Le Cann. 2005. Winter upper ocean circulation in the Western Iberian Basin—fronts, eddies and poleward flows: An overview. Deep Sea Res. Part I Oceanogr. Res. Pap. **52**: 621–646, doi:10.1016/j.dsr.2004.11.005.

Penven, P., P. Marchesiello, L. Debreu, and J. Lefèvre. 2008. Software tools for pre- and post-processing of oceanic regional simulations. Environ. Model. Softw. **23**: 660–662, doi:10.1016/j.envsoft.2007.07.004.

Periáñez, R., and F. Caravaca. 2010. A set of rapid-response models for pollutant dispersion assessments in southern Spain coastal waters. Mar. Pollut. Bull. **60**: 1412–1422, doi:10.1016/j.marpolbul.2010.05.016.

Phillips, B. F. and A. N. Sastry. 1980. Larval ecology. The Biology and Management of Lobsters. Vol. 2. Ecology and Management. P. 11–58. *In* J. S. Cobb and B. F. Phillips [eds.], Academic Press.

© 2013 by the Association for the Sciences of Limnology and Oceanography, Inc. / e-ISSN 2157-3689

Downloaded by guest on May 26, 2013

Pingree, R. D., and B. Le Cann. 1989. Celtic and Armorican slope and shelf residual currents. Prog. Oceanogr. **23**: 303–338, doi:10.1016/0079-6611(89)90003-7.

———, 1990. Structure, strength and seasonality of the slope currents in the Bay of Biscay region. J. Mar. Biol. Assoc. U.K. **70**: 857–885, doi:10.1017/S0025315400059117.

———, 1992. Three anticyclonic slope water oceanic eddies (SWODDIES) in the southern Bay of Biscay in 1990. Deep Sea Res. Part A Oceanogr. Res. Pap. **39** (7–8): 1147–1175.

Pous, S., E. Feunteun, and C. Ellien. 2010. Investigation of tropical eel spawning area in the south-western Indian Ocean: Influence of the oceanic circulation. Prog. Oceanogr. **86**: 396–413, doi:10.1016/j.pocean.2010.06.002.

Reverdin, G.,, P. P. Niiler, and H. Valdimarsson. 2003. North Atlantic Ocean surface currents. J. Geophys. Res. **108** (C1): 2-1–2-21, doi:10.1029/2001JC001020.

Richardson, P. L., and K. Mooney. 1975. The Mediterranean Outflow—a simple advection diffusion model. J. Phys. Oceanogr. **5**: 476–482, doi:10.1175/1520-0485(1975)005<0476:TMOSAD>2.0.CO;2.

Rodríguez, J. M., S. Hernández-León, and E. D. Barton. 1999. Mesoscale distribution of fish larvae in relation to an upwelling filament off northwest Africa. Deep-Sea Res. Oceanogr. Res. Pap. **46**: 1969–1984, doi:10.1016/S0967-0637(99)00036-9.

Rodríguez, J. M., M. Moyano, and S. Hernández-León. 2009. The ichthyoplankton assemblage of the Canaries–African Coastal Transition Zone: A review. Prog. Oceanogr. **83**: 314–321, doi:10.1016/j.pocean.2009.07.009.

Roughgarden, J., S. D. Gaines, and H. P. Possingham. 1988. Recruitment dynamics in complex life cycles. Science **241**: 1460–1466, doi:10.1126/science.11538249.

Sangrà, P., et al. 2009. The Canary Eddy Corridor: A major pathway for long-lived eddies in the subtropical North Atlantic. Deep Sea Res. Part I Oceanogr. Res. Pap. **56**: 2100–2114, doi:10.1016/j.dsr.2009.08.008.

Schmincke, H. U. 1973. Magmatic evolution and tectonic regime in the Canary, Madeira and Azores island groups. Bull. Geol. Soc. Am. **84**: 633–648, doi:10.1130/0016-7606(1973)84<633:MEATRI>2.0.CO;2.

Serra, N., and I. Ambar. 2002. Eddy generation in the Mediterranean Undercurrent. Deep Sea Res. Part II Top. Stud. Oceanogr. **49**: 4225–4243, doi:10.-01016/S0967645(02)00152-2.

Shchepetkin, A. F., and J. C. McWilliams. 2003. A method for computing horizontal pressure-gradient force in an oceanic model with a nonaligned vertical coordinate. J. Geophys. Res. **108** (C3): 3090, doi:10.1029/2001JC001047.

———, 2005. The Regional Oceanic Modeling System (ROMS): A split-explicit, free-surface, topography-following-coordinate oceanic model. Ocean Model. **9**: 347–404, doi:10.1016/j.ocemod.2004.08.002.

Song, Y., and D. Haidvogel. 1994. Numerical simulations of the CCS under the joint effects of coastal geometry and surface forcing. J. Comput. Phys. **115**: 228–244.

Sotillo, M. G., et al. 2008. Towards an operational system for oil-spill forecast over Spanish waters: Initial developments and implementation test. Mar. Pollut. Bull. **56**: 686–703, doi:10.1016/j.marpolbul.2007.12.021.

Stramma, L. 1984. Geostrophic transport in the warm water sphere of the eastern subtropical North Atlantic. J. Mar. Res. **42**: 537–558, doi:10.1357/002224084788506022.

Strathmann, R. R. 1985. Feeding and nonfeeding larval development and life-history evolution in marine invertebrates. Annu. Rev. Ecol. Syst. **16**: 339–361, doi:10.1146/annurev.es.16.110185.002011.

Sy, A. 1988. Investigation of large-scale circulation patterns in the central North Atlantic: The North Atlantic Current, the Azores Current, and the Mediterranean Water plume in the area of the Mid-Atlantic Ridge. Deep-Sea Res. **35**: 383–413, doi:10.1016/0198-0149(88)90017-9.

Thorson, G. 1950. Reproductive and larval ecology of marine bottom invertebrates. Biol. Rev. Camb. Philos. Soc. **25**: 1–45, doi:10.1111/j.1469-185X.1950.tb00585.x.

Valdivieso Da Costa, M., and B. Blanke. 2004. Lagrangian methods for flow climatologies and trajectory error assessment. Ocean Model. **6**: 335–358, doi:10.1016/S1463-5003(03)00023-4.

van Sebille, E., P. J. van Leeuwen, A. Biastoch, C. N. Barron, and W. P. M. de Ruijter. 2009. Lagrangian validation of numerical drifter trajectories using drifting buoys: Application to the Agulhas system. Ocean Model. **29**: 269–276, doi:10.1016/j.ocemod.2009.05.005.

Volkov, D., and L. Fu. 2010. On the reasons for the formation and variability of the Azores Current. J. Phys. Oceanogr. **40**: 2197–2220, doi:10.1175/2010JPO4326.1.

Watson, J. R., S. Mitarai, D. A. Siegel, J. E. Caselle, C. Dong, and J. C. McWilliams. 2010. Realized and potential larval connectivity in the Southern California Bight. Mar. Ecol. Prog. Ser. **401**: 31–48, doi:10.3354/meps08376.

Winston, J. E. 2012. Dispersal in marine organisms without a pelagic larval phase. Integr. Comp. Biol. **52**: 447–457, doi:10.1093/icb/ics040.

Xavier, J. R., R. W. van Soest, J. A. Breeuwer, A. M. Martins, and S. B. Menken. 2010. Phylogeography, genetic diversity and structure of the poecilosclerid sponge *Phorbas fictitius* at oceanic islands. Contrib. Zool. **79**: 119–129.

Received: 11 September 2012
Amended: 24 November 2012
Accepted: 29 January 2013

© 2013 by the Association for the Sciences of Limnology and Oceanography, Inc. / e-ISSN 2157-3689

Downloaded by guest on May 26, 2013